

Highlighting a study by a group of researchers led by Prof. Ya Du from Nanjing Tech University and Prof. Haishen Yang from Shanghai University of Electric Power.

Readily useable bulk phenoxazine-based covalent organic framework cathode materials with superior kinetics and high redox potentials

Two distinctive p-type phenoxazine-based COFs (DAPO-COFs) with high discharge potentials (up to 3.6 V vs. Li/Li⁺) are introduced as directly usable lithium ion battery cathode materials, i.e. without pre-composition with conductive additives or extra exfoliation. Pristine bulk DAPO-COFs are demonstrated as excellent cathode materials with superior active-site accessibility, ultrafast redox kinetics, and remarkable cycling stability.

As featured in:



See Haishen Yang, Ya Du *et al.*,
J. Mater. Chem. A, 2021, **9**, 10661.

Cite this: *J. Mater. Chem. A*, 2021, 9, 10661Received 5th November 2020
Accepted 22nd February 2021

DOI: 10.1039/d0ta10785a

rsc.li/materials-a

Readily useable bulk phenoxazine-based covalent organic framework cathode materials with superior kinetics and high redox potentials†

Zhiying Meng,^a Ying Zhang,^b Mengqing Dong,^a Yue Zhang,^a Fengmin Cui,^a Teck-Peng Loh,^{ac} Yinghua Jin,^{bd} Wei Zhang,^{bd} Haishen Yang^{de}*^b and Ya Du^{de}*^a

Redox-active covalent organic frameworks (COFs) with dense redox sites are promising electrical energy storage materials with robust architectures, high surface areas, insolubility in electrolytes, and open pores for electrolyte transportation. However, low redox potentials and poor electrical conductivity of pristine COFs often result in low accessibilities of redox-active sites and slow redox kinetics, greatly limiting their practical applications. Herein, we report the design and synthesis of two novel p-type phenoxazine-based COFs (DAPO-COFs) with high redox potentials (~ 3.6 V vs. Li/Li⁺) and excellent electrical conductivities. Simply blended with conductive additives (CAs) and binders, pristine bulk DAPO-COFs without pre-composition with CAs or extra exfoliation are readily useable as cathode materials for lithium-ion batteries. Both as-synthesized DAPO-COF powders displayed superior active-site accessibility, ultrafast redox kinetics, and remarkable cycling stability. This work provides new perspectives on the development of readily useable COF-based cathode materials, and contributes to the advancement of eco-friendly and sustainable organic-based energy storage devices.

Two-dimensional covalent organic frameworks (2D COFs) represent a novel class of predesignable porous crystalline polymers with various applications. With redox-active molecules as building blocks, robust redox-active COFs could be precisely achieved with dense redox sites, enhanced electrochemical stability, insolubility in organic solvents (*i.e.* electrolytes), and tunable open pores for mass transportation.^{1–8} Redox-active COFs have many advantages as an emerging type

of sustainable organic electrode materials. To date, a number of COFs with different redox-active groups have been explored as electrode materials.^{9–24} However, most as-prepared bulk COF powders exhibit rather low active-site accessibility and slow redox kinetics because of their extremely low bulk electrical conductivities.^{11,25–27} Significant efforts have been devoted to improving their electrical conductivities through sophisticated thin-film formation or exfoliation strategies or *in situ* preparation of COF composites.^{15,28–33} However, numerous drawbacks of those approaches, such as complicated manipulations, poor scalability, energy capacity deductions, *etc.*, limit their practical applications. Therefore, readily useable bulk COFs with high electrical conductivities are highly desired.³⁴ Moreover, most known COFs have operating voltages lower than 3.0 V,^{15,27,35,36} and thus COFs with high redox potentials are also highly desired. Herein, we successfully address these problems by construction of novel p-type phenoxazine-based COFs (DAPO-COFs) with high working potentials (~ 3.6 V vs. Li/Li⁺), fast redox kinetics, and ready bulk usability (Scheme 1).

DAPO-TFB-COF and DAPO-TpOMe-COF (DAPO-COFs) were synthesized through the condensation of 2,7-diamine-10-methyl-phenoxazine (DAPO) with 1,3,5-triformylbenzene (TFB) and 2,4,6-trimethoxy-1,3,5-triformylbenzene (TpOMe), respectively (Scheme 1). Both DAPO-COFs were characterized by FT-IR,



Scheme 1 Design and synthesis of DAPO-COFs.

^aInstitute of Advanced Synthesis, School of Chemistry and Molecular Engineering, Nanjing Tech University, Nanjing 211816, China. E-mail: teckpeng@njtech.edu.cn; ias_ydu@njtech.edu.cn

^bShanghai Key Laboratory of Materials Protection and Advanced Materials in Electric Power, Shanghai University of Electric Power, Shanghai 200090, China. E-mail: yanghsh@shiep.edu.cn

^cDivision of Chemistry and Biological Chemistry, School of Physical and Mathematical Sciences, Nanyang Technological University, Singapore 637616, Singapore

^dDepartment of Chemistry, University of Colorado, Boulder, CO 80309, USA

† Electronic supplementary information (ESI) available. See DOI: 10.1039/d0ta10785a

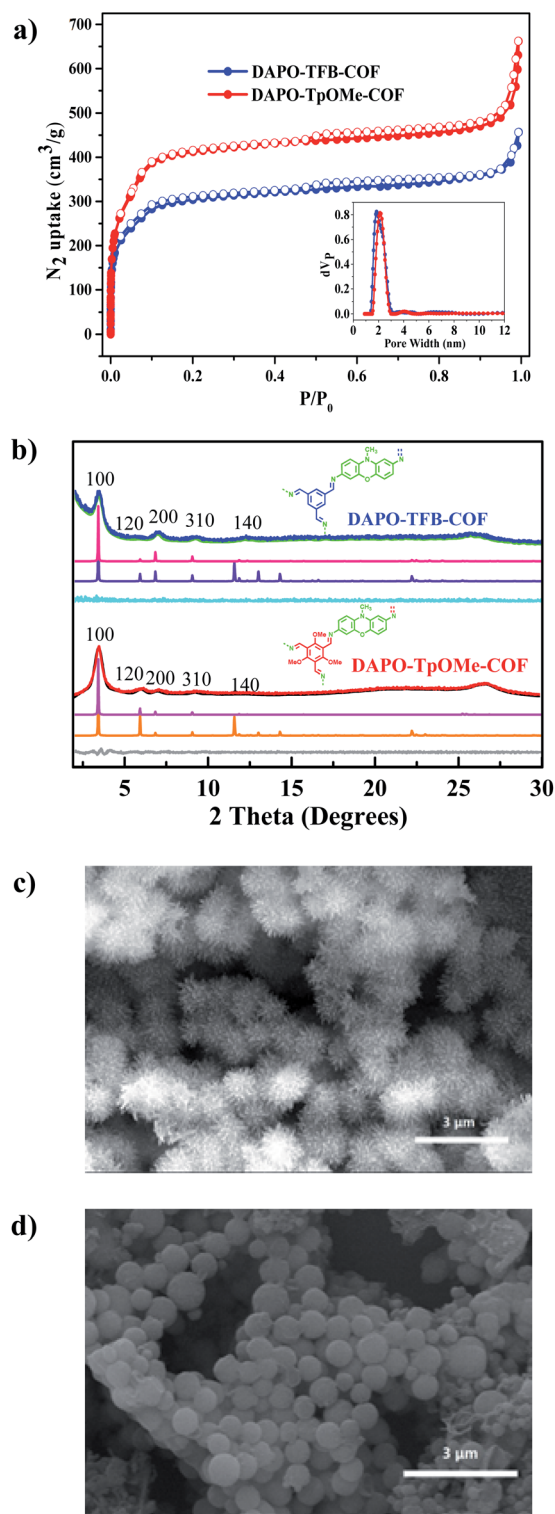


Fig. 1 (a) Nitrogen adsorption–desorption isotherms of DAPO-COFs and QSDFT pore size distributions of DAPO-COFs (inset); (b) experimental PXRD patterns (blue), Pawley refined patterns (green), difference plots (cyan), simulated AA-stacking patterns (pink), and simulated AB-stacking patterns (violet) for DAPO-TFB-COF and experimental PXRD patterns (red), Pawley refined patterns (black), difference plots (grey), simulated AA-stacking patterns (purple), and simulated AB-stacking patterns (orange) for DAPO-TpOMe-COF; (c) SEM image of DAPO-TFB-COF at 3 μm scale; (d) SEM image of DAPO-TpOMe-COF at 3 μm scale.

¹³C CP/MAS NMR, elemental analysis (EA), TGA, SEM and PXRD analysis. FT-IR spectra of DAPO-TFB-COF and DAPO-TpOMe-COF show the presence of the stretching bands of C=N at 1514 cm⁻¹ and 1592 cm⁻¹, respectively, and the disappearance of the typical stretching bands of carbonyl (>C=O) and amino groups (-NH₂) of starting materials, indicating the successful formation of imine bonds (Fig. S2†). In the solid-state cross-polarization magic-angle spinning ¹³C NMR spectra, we observed the peak corresponding to the imine carbons (C=N) at 153 ppm for DAPO-TFB-COF, and 152 ppm for DAPO-TpOMe-COF (Fig. S3†). Thermogravimetric analyses show that both DAPO-TFB-COF and DAPO-TpOMe-COF have excellent thermal stability, losing only 8% and 12%, respectively, at the temperature of 450 °C (Fig. S6†). High thermal stability of electrode materials is critical for electrochemical energy storage devices (EESDs) under high-temperature conditions. Scanning electron microscopy (SEM) images of both DAPO-COFs show uniform granular aggregates with diameters of several hundred nanometers (Fig. 1c and d).

The crystallinity of DAPO-TFB-COF and DAPO-TpOMe-COF was examined by powder X-ray diffraction (PXRD) measurement (Fig. 1b). The diffraction peaks at 3.49°, 5.86°, 6.82°, 9.26° and 12.22° for DAPO-TFB-COF correspond to the reflections of (100), (120), (200), (310) and (140) diffractions, and the diffraction peaks at 3.54°, 6.04°, 7.06°, 9.16° and 12.13° for DAPO-TpOMe-COF are attributed to the reflections of (100), (120), (200), (310) and (140) facets. The experimental PXRD patterns of both frameworks are consistent with the simulated AA stacking models calculated using Materials Studio software. Pawley refinement results show that the differences between experimental and simulated data are negligible with reasonable *R*_{wp} and *R*_p values (6.43% and 5.05% for DAPO-TFB-COF; 4.49% and 3.37% for DAPO-TpOMe-COF). The slightly broad PXRD peaks might be due to the rotational freedom of DAPO with a rather low symmetry, which likely causes imperfection in crystallinity. The porosity of DAPO-TFB-COF and DAPO-TpOMe-COF was investigated by N₂ adsorption–desorption isotherms as shown in Fig. 1a. The BET surface areas were calculated to be 1151 m² g⁻¹ and 1662 m² g⁻¹ for DAPO-TFB-COF and DAPO-TpOMe-COF, respectively. The simulated surface areas based on the crystal structure are 2434 and 2033 m² g⁻¹, respectively. The lower experimental BET surface area than the theoretical values is likely due to the imperfect crystalline structures. Calculations based on the quenched solid density functional theory (QSDFT) show narrow pore-size distribution (PSD) centered around 1.9 nm for DAPO-TFB-COF and 2.1 nm for DAPO-TpOMe-COF, which matches reasonably well with the theoretical values (2.3 nm for DAPO-TFB-COF and 2.3 nm for DAPO-TpOMe-COF) of the eclipsed stacking structures. High specific surface areas would be beneficial for the active-site accessibility, while uniform large pores render DAPO-COFs with the ability to hold sufficient electrolytes and the pathway for ion transport.³⁷

The electrochemical performance of DAPO-COFs as cathode active materials was evaluated in 2016 coin-type cells. The cyclic voltammetry (CV) curves are shown in Fig. 2a. DAPO-TpOMe-COF (red) shows two distinctive oxidation peaks I and II in the potential region of 3.4–4.0 V, while DAPO-TFB-COF (blue)

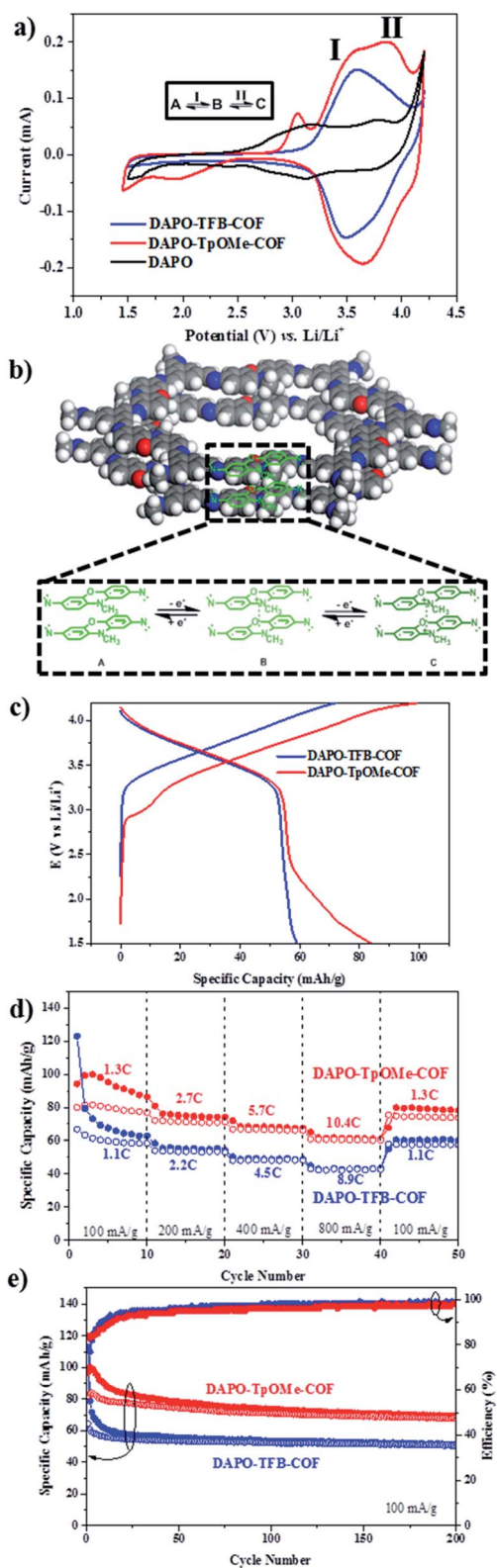


Fig. 2 (a) CV curves with a scan rate of 1 mV s^{-1} ; (b) π - π interaction and redox processes of DAPO-COFs; (c) charge (filled) and discharge (empty) curves at 100 mA g^{-1} ; (d) rate performance at different applied discharge C-rates; (e) cycling stability and coulombic efficiency at 100 mA g^{-1} .

shows one oxidation peak with a very gentle slope in the potential region of 3.6–4.0 V, indicating that an overlapped peak is present.

The broad reduction peaks of both DAPO-COFs imply the presence of overlapped peaks. The CV curves, which are quite different from that of the parent phenoxazine, suggest a step-wise charge storage mechanism.^{38,39} This observation could be reasonably explained by the strong interlayer π - π interaction and the formation of a stabilized intermediate state B upon oxidation, in which the phenoxazine radical cation formed in one layer can associate with the adjacent neutral phenoxazine unit in the neighboring layer (Fig. 2b).³⁸ The peak pair I between 3.38 and 3.62 V corresponds to the transition between states A and B, while the peak pair II between 3.68 and 3.85 V corresponds to the transition between states B and C. The result also indicates the efficient interlayer charge-carrier transportation. The more intensive peak pair II in DAPO-TpOMe-COF (red) than that in DAPO-TFB-COF (blue) might indicate the more efficient transition between states B and C and more intense interlayer interactions of the oxidized states. This difference could be attributed to the presence of methoxy groups on the linker, which also accounts for the redox peaks at the potential regions of 1.5–3.2 V, providing extra capacity for the framework. A molecular model compound (TpOMe-Ami) was prepared to explore the redox mechanism (Section B, ESI†). TpOMe-Ami showed small redox peaks at the potential regions of 1.5–3.2 V, as well as the main redox peaks between 3.2 V and 4.0 V (Fig. S7†). Furthermore, the introduction of electron-donating groups on the linker also provides the COF material with superior kinetics of charge transfer, as evidenced by electrochemical impedance spectroscopy (EIS). The charge transfer resistance (R_{ct}) of DAPO-TpOMe-COF is 161 ohm, which is less than that of DAPO-TFB-COF (201 ohm) (Fig. S8†). Both COF powders were pressed into disc-shaped pellets ($\varnothing = 1 \text{ cm}$) with a thickness of 0.22 mm, and the conductivity test was performed at room temperature. The conductivities of DAPO-TFB-COF and DAPO-TpOMe-COF bulk pellets were measured to be $5.35 \times 10^{-7} \text{ S cm}^{-1}$ and $1.28 \times 10^{-5} \text{ S cm}^{-1}$, respectively.

Both COFs exhibit high operating potentials and high redox reversibility. The gaps between each pair of oxidation and reduction peaks of DAPO-COFs are pretty narrow, especially for the peak pair I ($\sim 0.1 \text{ V}$), indicating the excellent electrical conductivity.³⁰ Also, the narrow redox peak separations reflect the rapid redox kinetics during charge and discharge processes. These observations are attributed to the synergistic effect of the peculiar properties of the *N*-substituted phenoxazine motif and the unique COF architectures.

The charge-storage capabilities of DAPO-COFs were further evaluated with galvanostatic charge-discharge measurements in the potential range of 1.5–4.2 V (vs. Li/Li⁺) at a current density of 100 mA g^{-1} (Fig. 2c). The charge-discharge curves of DAPO-TFB-COF and DAPO-TpOMe-COF are in good accordance with their CV results. Pristine DAPO-TpOMe-COF provides high first discharge specific capacity up to 81.9 mA h g^{-1} , including the capacity below 3.1 V ($\sim 10 \text{ mA h g}^{-1}$), possibly originating from the TpOMe linker. Pristine DAPO-TFB-COF delivered a capacity of 64.4 mA h g^{-1} , which corresponds to 72% utilization of the

theoretical redox-active sites. The utilization efficiency of active-sites of both pristine DAPO-COFs is higher than that of most of the known COFs used as cathode materials, and comparable to or even better than their composites prepared *in situ* with conductive additives.^{16,18,27} The rapid decay of charge capacities of DAPO-COFs in the initial cycles is possibly due to the SEI film formation and growth, and/or the dissolution of trace amounts of electrode materials.^{40,41}

Both pristine DAPO-COFs demonstrate excellent rate performances. As shown in Fig. 2d, when the current densities increased from 100 mA g⁻¹ to 800 mA g⁻¹, DAPO-TFB-COF and DAPO-TpOMe-COF retain a reversible capacity up to 43.1 mA h g⁻¹ and 61.0 mA h g⁻¹, respectively, which correspond to 65% and 76% of their initial capacity values of 66.8 mA h g⁻¹ and 80.0 mA h g⁻¹, respectively, at 100 mA g⁻¹. When the current density was set back to 100 mA g⁻¹, high specific capacities of 58.0 mA h g⁻¹ and 75.5 mA h g⁻¹ were attained for DAPO-TFB-COF and DAPO-TpOMe-COF, respectively, corresponding to 87% and 94% of their respective initial capacities. DAPO-TpOMe-COF is superior to DAPO-TFB-COF in rate capability.

Remarkably, both pristine DAPO-COFs demonstrate robust long-term cycling stabilities, as shown in Fig. 2e and S1a.† When evaluated at a current density of 100 mA g⁻¹, the capacities of DAPO-TpOMe-COF and DAPO-TFB-COF are 68.0 mA h g⁻¹ and 51.0 mA h g⁻¹ with high initial capacity retentions of 79% and 87%, respectively, after 200 cycles. Even after 1000 cycles at the current density of 100 mA g⁻¹, DAPO-TFB-COF still retains 72% of its initial capacity. The coulombic efficiencies for both DAPO-COFs are higher than 99%, indicating that there are almost no capacity losses during the charge and discharge processes. We found that the crystallinity of the COF samples has a noticeable effect on their energy storage performance. As shown in Fig. S1b and c,† the amorphous sample of DAPO-TFB-COF exhibits much lower specific capacity compared to the crystalline sample. In our hands, the COF samples were obtained only with decent crystallinity likely due

to the DAPO building blocks with relatively low symmetry. Further improvement of electrochemical performance of DAPO-COFs as cathode materials is anticipated if higher crystallinity of the samples can be achieved.

In order to have a better understanding of their excellent performance, the surface morphologies of the electrode materials were examined using SEM images before and after cycling (Fig. 3). As shown in the SEM images before cycling, the conductive carbons and COF aggregates distribute irregularly after the insufficient ball-milling. The COFs almost retained their original sizes and morphologies and there are clear interfaces between neighboring particles (Fig. 3a and c). Surprisingly, after cycling, the boundaries between the particles disappeared, and all the particles were “concreted” together. It appears that the COF spherical particles are “solidified”, and conductive carbon particles are wrapped up and indistinguishable. The cross-section electrode SEM images confirmed similar observations (Fig. S9 and S10†). Previously, a similar morphology change was observed for a p-type linear poly(vinylphenothiazine)-based cathode material, which was affirmed to be through a deposition/dissolution mechanism.⁴² However, since DAPO-COFs are insoluble in the electrolytes, even in their oxidized (charged) states, such a mechanism is not applicable in the present case. Although disappearance of the boundaries of cathode material particles was observed for the first time for COF-based electrode materials and a clear mechanism remains elusive, such a boundary self-bridging property would be an efficient approach to improve the performance of electrode materials.

In conclusion, we have successfully developed two novel p-type redox-active COFs (DAPO-COFs) with high discharge potentials (~3.6 V vs. Li/Li⁺), high crystallinity, regular pore channels and high surface areas. The pristine DAPO-COFs are readily useable in bulk as excellent cathode materials by simply mixing with conductive agents and binders as usual for lithium-ion batteries. Both pristine DAPO-COFs exhibit remarkable rate capabilities, ultra-high active-site utilization, and outstanding cycling stabilities. DAPO-TpOMe-COF with an electron-donating methoxy group functionalized linker (TpOMe) exhibits superior above-mentioned performances to those of DAPO-TFB-COF. Our study indicates that, in addition to the redox functional motifs, the performance of COFs could be finely tuned by linker modifications. This work provides a general approach to develop bulk useable COF-based cathode materials of high performance for the advancement of eco-friendly and sustainable organic-based energy storage devices.

Conflicts of interest

There are no conflicts to declare.

Acknowledgements

Y. D. acknowledges financial support from the National Natural Science Foundation of China (21805134), Natural Science Foundation of Jiangsu Province, China (BK20191363), Science and Technology Innovation Project for Overseas Students from

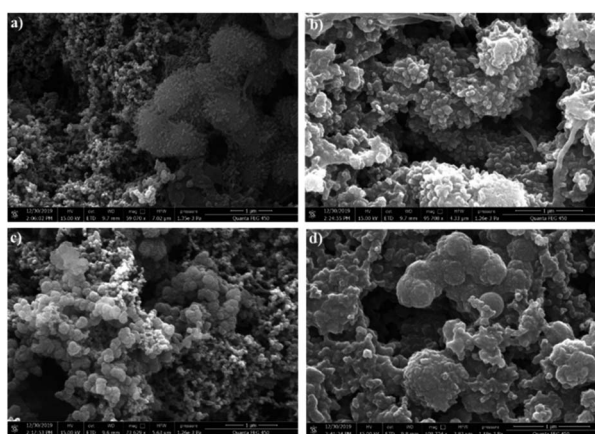


Fig. 3 SEM images of (a) electrode with DAPO-TFB-COF before cycling; (b) electrode with DAPO-TFB-COF after cycling; (c) electrode with DAPO-TpOMe-COF before cycling; (d) electrode with DAPO-TpOMe-COF after cycling.

Nanjing City, and Start-up Grant No. 39837141 from NJTECH. H. Y. is thankful for the financial support from the Science and Technology Commission of Shanghai Municipality (19DZ2271100), and Program for Professor of Special Appointment (Eastern Scholar) at Shanghai Institutions of Higher Learning. The authors thank Prof. Xin Zhao and Mrs Qiaoyan Qi for their assistance with the PXRD simulation.

Notes and references

- 1 A. P. Côté, A. I. Benin, N. W. Ockwig, M. O'Keeffe, A. J. Matzger and O. M. Yaghi, *Science*, 2005, **310**, 1166–1170.
- 2 H. M. El-Kaderi, J. R. Hunt, J. L. Mendoza-Cortés, A. P. Côté, R. E. Taylor, M. O'Keeffe and O. M. Yaghi, *Science*, 2007, **316**, 268–272.
- 3 S.-Y. Ding and W. Wang, *Chem. Soc. Rev.*, 2013, **42**, 548–568.
- 4 X. Feng, X. Ding and D. Jiang, *Chem. Soc. Rev.*, 2012, **41**, 6010–6022.
- 5 D. N. Bunck and W. R. Dichtel, *Angew. Chem., Int. Ed.*, 2012, **51**, 1885–1889.
- 6 J. W. Colson and W. R. Dichtel, *Nat. Chem.*, 2013, **5**, 453–465.
- 7 G. Wang, N. Chandrasekhar, B. P. Biswal, D. Becker, S. Paasch, E. Brunner, M. Addicoat, M. Yu, R. Berger and X. Feng, *Adv. Mater.*, 2019, **31**, 1901478.
- 8 Y. Li, W. Chen, G. Xing, D. Jiang and L. Chen, *Chem. Soc. Rev.*, 2020, **49**, 2852–2868.
- 9 L. Zhou, K. Zhang, Z. Hu, Z. Tao, L. Mai, Y.-M. Kang, S.-L. Chou and J. Chen, *Adv. Energy Mater.*, 2018, **8**, 1701415.
- 10 H. Yang, S. Zhang, L. Han, Z. Zhang, Z. Xue, J. Gao, Y. Li, C. Huang, Y. Yi, H. Liu and Y. Li, *ACS Appl. Mater. Interfaces*, 2016, **8**, 5366–5375.
- 11 S. Haldar, K. Roy, S. Nandi, D. Chakraborty, D. Puthusseri, Y. Gawli, S. Ogale and R. Vaidhyanathan, *Adv. Energy Mater.*, 2018, **8**, 1702170.
- 12 Z. Wang, Y. Li, P. Liu, Q. Qi, F. Zhang, G. Lu, X. Zhao and X. Huang, *Nanoscale*, 2019, **11**, 5330–5335.
- 13 S. Chandra, D. Roy Chowdhury, M. Addicoat, T. Heine, A. Paul and R. Banerjee, *Chem. Mater.*, 2017, **29**, 2074–2080.
- 14 X. Chen, Y. Li, L. Wang, Y. Xu, A. Nie, Q. Li, F. Wu, W. Sun, X. Zhang, R. Vajtai, P. M. Ajayan, L. Chen and Y. Wang, *Adv. Mater.*, 2019, **31**, 1901640.
- 15 S. Wang, Q. Wang, P. Shao, Y. Han, X. Gao, L. Ma, S. Yuan, X. Ma, J. Zhou, X. Feng and B. Wang, *J. Am. Chem. Soc.*, 2017, **139**, 4258–4261.
- 16 X. Chen, H. Zhang, C. Ci, W. Sun and Y. Wang, *ACS Nano*, 2019, **13**, 3600–3607.
- 17 F. Xu, X. Chen, Z. Tang, D. Wu, R. Fu and D. Jiang, *Chem. Commun.*, 2014, **50**, 4788–4790.
- 18 S. Feng, H. Xu, C. Zhang, Y. Chen, J. Zeng, D. Jiang and J.-X. Jiang, *Chem. Commun.*, 2017, **53**, 11334–11337.
- 19 Y. Hu, N. Dunlap, S. Wan, S. Lu, S. Huang, I. Sellinger, M. Ortiz, Y. Jin, S.-h. Lee and W. Zhang, *J. Am. Chem. Soc.*, 2019, **141**, 7518–7525.
- 20 S. Gu, S. Wu, L. Cao, M. Li, N. Qin, J. Zhu, Z. Wang, Y. Li, Z. Li, J. Chen and Z. Lu, *J. Am. Chem. Soc.*, 2019, **141**, 9623–9628.
- 21 C. R. DeBlase, K. E. Silberstein, T. T. Truong, H. D. Abruna and W. R. Dichtel, *J. Am. Chem. Soc.*, 2013, **135**, 16821–16824.
- 22 M. Li, J. Liu, Y. Li, G. Xing, X. Yu, C. Peng and L. Chen, *CCS Chem.*, 2020, **2**, 696–706.
- 23 J. Liu, Y. Zhou, Z. Xie, Y. Li, Y. Liu, J. Sun, Y. Ma, O. Terasaki and L. Chen, *Angew. Chem., Int. Ed.*, 2020, **59**, 1081–1086.
- 24 Q. Jiang, P. Xiong, J. Liu, Z. Xie, Q. Wang, X.-Q. Yang, E. Hu, Y. Cao, J. Sun, Y. Xu and L. Chen, *Angew. Chem., Int. Ed.*, 2020, **59**, 5273–5277.
- 25 S. N. Talapaneni, T. H. Hwang, S. H. Je, O. Buyukcakir, J. W. Choi and A. Coskun, *Angew. Chem., Int. Ed.*, 2016, **55**, 3106–3111.
- 26 W. Liu, X. Luo, Y. Bao, Y. P. Liu, G.-H. Ning, I. Abdelwahab, L. Li, C. T. Nai, Z. G. Hu, D. Zhao, B. Liu, S. Y. Quek and K. P. Loh, *Nat. Chem.*, 2017, **9**, 563–570.
- 27 D.-H. Yang, Z.-Q. Yao, D. Wu, Y.-H. Zhang, Z. Zhou and X.-H. Bu, *J. Mater. Chem. A*, 2016, **4**, 18621–18627.
- 28 C. R. Mulzer, L. Shen, R. P. Bisbey, J. R. McKone, N. Zhang, H. D. Abruna and W. R. Dichtel, *ACS Cent. Sci.*, 2016, **2**, 667–673.
- 29 J. Sun, A. Klechikov, C. Moise, M. Prodana, M. Enachescu and A. V. Talyzin, *Angew. Chem., Int. Ed.*, 2018, **57**, 1034–1038.
- 30 F. Xu, S. Jin, H. Zhong, D. Wu, X. Yang, X. Chen, H. Wei, R. Fu and D. Jiang, *Sci. Rep.*, 2015, **5**, 8225.
- 31 H. Wu, Q. Meng, Q. Yang, M. Zhang, K. Lu and Z. Wei, *Adv. Mater.*, 2015, **27**, 6504–6510.
- 32 Z. Lei, Q. Yang, Y. Xu, S. Guo, W. Sun, H. Liu, L.-P. Lv, Y. Zhang and Y. Wang, *Nat. Commun.*, 2018, **9**, 576.
- 33 Y. Yusran, H. Li, X. Guan, D. Li, L. Tang, M. Xue, Z. Zhuang, Y. Yan, V. Valtchev, S. Qiu and Q. Fang, *Adv. Mater.*, 2020, **32**, 1907289.
- 34 E. Vitaku, C. N. Gannett, K. L. Carpenter, L. Shen, H. D. Abruna and W. R. Dichtel, *J. Am. Chem. Soc.*, 2020, **142**, 16–20.
- 35 F. Xu, H. Xu, X. Chen, D. Wu, Y. Wu, H. Liu, C. Gu, R. Fu and D. Jiang, *Angew. Chem., Int. Ed.*, 2015, **54**, 6814–6818.
- 36 C. R. DeBlase, K. Hernández-Burgos, J. M. Rotter, D. J. Fortman, D. dos S. Abreu, R. A. Timm, I. C. N. Diógenes, L. T. Kubota, H. D. Abruna and W. R. Dichtel, *Angew. Chem., Int. Ed.*, 2015, **54**, 13225–13229.
- 37 Y. Li, Z. Ding, X. Zhang, J. Li, X. Liu, T. Lu, Y. Yao and L. Pan, *J. Mater. Chem. A*, 2019, **7**, 25305–25313.
- 38 M. Kolek, F. Otteny, P. Schmidt, C. Mück-Lichtenfeld, C. Einholz, J. Becking, E. Schleicher, M. Winter, P. Bieker and B. Esser, *Energy Environ. Sci.*, 2017, **10**, 2334–2341.
- 39 F. Otteny, V. Perner, D. Wassy, M. Kolek, P. Bieker, M. Winter and B. Esser, *ACS Sustainable Chem. Eng.*, 2020, **8**, 238–247.
- 40 S. Chen, T. Jia, G. Zhou, C. Zhang, Q. Hou, Y. Wang, S. Luo, G. Shi and Y. Zeng, *J. Electrochem. Soc.*, 2019, **166**, A2543–A2548.
- 41 M. Rajesh, F. Dolhem, C. Davoisne and M. Becuwe, *ChemSusChem*, 2020, **13**, 2364–2370.
- 42 M. Kolek, F. Otteny, J. Becking, M. Winter, B. Esser and P. Bieker, *Chem. Mater.*, 2018, **30**, 6307–6317.